

Enabling cooperative adaptive cruise control on strings of vehicles with heterogeneous dynamics and powertrains

Carlos Flores, John Spring, David Nelson, Simeon Iliev & Xiao-Yun Lu

To cite this article: Carlos Flores, John Spring, David Nelson, Simeon Iliev & Xiao-Yun Lu (2022): Enabling cooperative adaptive cruise control on strings of vehicles with heterogeneous dynamics and powertrains, Vehicle System Dynamics, DOI: [10.1080/00423114.2022.2042568](https://doi.org/10.1080/00423114.2022.2042568)

To link to this article: <https://doi.org/10.1080/00423114.2022.2042568>



Published online: 01 Mar 2022.



Submit your article to this journal [↗](#)



View related articles [↗](#)



View Crossmark data [↗](#)



Enabling cooperative adaptive cruise control on strings of vehicles with heterogeneous dynamics and powertrains

Carlos Flores^a, John Spring^a, David Nelson^a, Simeon Iliev^b and Xiao-Yun Lu^{a,c}

^aPartners for Advanced Transportation Technology (PATH), University of California Berkeley, Richmond, CA, USA; ^bArgonne National Laboratory, Lemont, IL, USA; ^cLawrence Berkeley National Laboratory, Richmond, CA, USA

ABSTRACT

Recent studies have shown that positive impact of Cooperative Adaptive Cruise Control (CACC) can only be guaranteed as market penetration rate increases. Removing the string homogeneity constraint is essential to encourage widespread adoption. In this work, a hierarchical architecture is proposed to enable CACC on vehicles with not only mixed dynamics but also different powertrain types. A low-level layer deals with the vehicle and powertrain dynamics to provide accurate and consistent reference speed tracking response. The high-level layer uses: (1) a Linear Parameter Varying feedback system to provide loop stability, robustness and enforce a variable time gap policy and (2) a feedforward system that processes Vehicle-to-Vehicle information to enhance string stability and response bandwidth, by dealing with the string heterogeneity. A gap management strategy is built on top of the CACC architecture to handle gap setting changes or cut-in/out situations, via a dynamics constrained time gap trajectory planning algorithm. The proposed work has been designed, developed and validated on three different real passenger vehicles on public highways and test tracks, showing the potential of the proposed algorithm to enable robust string stable CACC, despite the different dynamics and powertrains considered.

ARTICLE HISTORY

Received 16 July 2021
Revised 18 October 2021
Accepted 30 December 2021

KEYWORDS

Cooperative adaptive cruise control; connected automated vehicles; heterogeneous strings; robust optimal control; vehicle dynamics control

1. Introduction

In recent years, interest for road vehicle automation has increased significantly. For instance, Adaptive Cruise Control (ACC) systems adoption is growing rapidly among commercial vehicles. These systems enhance driver comfort by relieving the gap regulation task to the ACC system. The vehicle is equipped with full longitudinal actuation capabilities and range measurement sensor (usually radar) to perform car-following. Nevertheless, several works have shown that commercially available ACC systems do not satisfy the string stability condition [1], which requires speed disturbances to not be amplified as they propagate in upstream direction [2]. Risky situations may arise from strong braking of downstream vehicles, due to the amplifying disturbance propagation, potentially producing rear-end collisions. Although setting a larger gap may reduce the disturbance amplifications, this harms traffic capacity and throughput.

A solution to disturbance amplification and traffic shockwaves caused by unstable car-following behaviours has been demonstrated via intelligent automated car-following algorithms [3], where ring experiments were performed with real vehicles to demonstrate its effectiveness. Even though these strategies are encouraging, the perception horizon remains limited to the immediately preceding vehicle. By augmenting the system perception with wireless Dedicated Short Range Communication (DSRC) links, one enables access to non-perceivable variables from not only the preceding vehicle but also forward vehicles.

The addition of DSRC to establish Vehicle-to-Vehicle (V2V) communication links is used on top of the automated car-following layer. This is the framework of platooning, which has demonstrated to allow very short constant distance gaps with stable car-following [4]. With these short gaps, not only the traffic capacity is increased, but also aerodynamic drafting is possible, reducing fuel consumption up to 17% [5] for heavy-duty trucks. However, its implementation has been restricted to high speed operation on dedicated lanes, avoiding large speed fluctuations or interaction with other non-equipped vehicles [6]. Since these requirements would hinder widespread adoption and implementation of platooning, Cooperative-ACC (CACC) has been introduced as a more flexible and cooperative framework, attracting a lot of attention in recent years.

CACC systems rely on V2V links with longitudinal automation and ranging sensors. They propose a more flexible framework with inter-distances proportional to the vehicle speed, i.e. Constant Time Gap (CTG) policy. Some results have shown safe and string stable operation with good disturbances rejection [7,8]. Studies have shown that CACC potentially increases traffic capacity and mobility, with the condition that high market penetration is reached [9]. Almost all CACC systems have been implemented on strings of identical vehicles, simplifying the deployment by replicating the system on every controlled vehicle. However, this requirement highly restricts the formation of CACC strings on road environments. To further encourage adoption of this technology and increase its positive impact, the constraint of string homogeneity should be overcome to permit CACC among non-identical vehicles. This increases the system complexity for two reasons: (1) different responses are observed to the same input or stimulus, hindering the replication of car-following system on all controlled vehicles, and (2) the study of upstream disturbances propagation is dependent on each vehicle dynamics and implemented control structure. In addition, variables as spacing errors or control actions are no longer valid for analysing string stability on heterogeneous formations, since these are closely related to each vehicle control structure [10]. For this reason, either longitudinal acceleration, speed or position evolution can be used to analyse string stability.

In the literature, several works have been proposed considering cooperative control of mixed vehicles. Projects as SARTRE [11] or the Grand Cooperative Driving Challenge (GCDG) in its two editions [12], have contributed to the logistics and V2V network implementation perspective. Interaction between CAVs and human-driven vehicles has also been considered [13] and demonstrated in real experiments, where variables from several forward vehicles are leveraged to enhance the car-following behaviour and even stabilising traffic shockwaves. Other works have focused on extending the control capabilities using consensus-based strategies [14], Model Predictive Control [15], adaptive optimal control [16], among others. A multi-model adaptive control method has been proposed in [17]. Shaw and Hedrick [18] studied a Leader-Predecessor Following (LPF) topology

strategy to ensure bounded spacing errors. Feedback with Proportional Derivative [19] or \mathcal{H}_∞ [20] controllers is of the most common methods used for CACC robust to string heterogeneity, used on either Predecessor-Following (PF) or LPF topologies. Nevertheless, these works are either validated on simulation results or through very conservative experiments. In addition, vehicle masses and sizes have been considered as the unique sources of dynamics heterogeneity on these works. To the best of our knowledge, there is no work that considers the problem of CACC implementation on a string with vehicles of different powertrain types, e.g. hybrid, electric, Internal Combustion Engine (ICE).

Another important aspect that hinders the public adoption of CACC is the risk of cutting-in vehicles. In [7], a two-controller strategy has been proposed to address the gap closing/opening required by cut-ins. A framework to handle cutting-in vehicles in CACC strings was proposed in [21], where the time gap changes linearly to open the spacing gap towards the cutting-in vehicle. Although promising results have been demonstrated, there is still room for improvement to guarantee a dynamics-constrained manoeuvring to safely handle these situations.

1.1. Motivation and contributions

This research work is motivated by the necessity to design more robust and adaptable control structures that allow high performance CACC on heterogeneous strings. It is also encouraged by the possibility to further improve the handling of cutting-in vehicles within strings of CACC vehicles. Further work needs to be done to demonstrate that strictly string stable CACC is feasible on strings of heterogeneous dynamics. In addition, the implementation and validation of CACC algorithms over real heterogeneous vehicle platforms are still missing to really test the performance limits, not only on test tracks but also over highway traffic situations. Such performance study would permit to assess the systems potential impact real traffic flow. This work targets these motivations by proposing a hierarchical control architecture that increases the CACC capabilities and its positive impact on traffic flow, considering vehicles of heterogeneous dynamics and powertrains. The following contributions are highlighted for this work:

- Analysis on the implications of dynamics heterogeneity on CACC strings of vehicles
- Guarantee of consistent reference speed tracking system for any vehicle type
- Generic feedforward-feedback architecture designed to be adapted with target time gap changes and robust string stability
- Handling of cutting-in vehicles within CACC strings using a dynamics-constrained trajectory planning of desired time gap
- Experimental validation of the proposed architecture on real vehicles of different dynamics and powertrains, including tests both on tracks and highway traffic.

This work proposes a hierarchical control architecture adaptable to different types of road vehicle dynamics and allows short time gap following with string stable performance. It is composed by a hierarchical structure of two layers. The low-level layer deals with the vehicle longitudinal dynamics and its actuators to track the desired reference speed. The high-level control layer processes the received V2V information from forward vehicles and controls the vehicle kinematics to regulate the gap towards preceding vehicle, with respect

to an adopted spacing policy. On top of this architecture, a gap management algorithm handles the desired gap settings or possible cutting-in vehicles. The proposed architecture can also be used under different communication topologies and can be adapted online to improve car-following performance given the dissimilarities between vehicles' dynamics. Extensive testing is done in public traffic with a three-vehicle CACC string to assess the system performance and test its limits. The rest of the paper is as follows. Section 2 presents the vehicle platforms setup, as well as the controlled string configuration. In Section 3, both layers of the generic control architecture are detailed. The gap management algorithm that governs the gap settings and generates the motion planning trajectory is described in Section 4. The experimental results that validate the robustness and benefits of the proposed architecture are showed in Section 5, for both test tracks and highways. Finally, the concluding remarks that derive from the proposed work and obtained results are provided in Section 6, followed by possible future work insights.

2. Vehicles experimental setup

The proposed architecture has been developed for three automated vehicles of different makes and powertrains. These are equipped with production ACC systems, which use: (1) wheel encoders to sense the vehicle longitudinal speed, (2) radar sensors to measure the clearance towards forward vehicles, (3) electronically reachable actuators, or drive-by-wire capabilities, and (4) embedded ACC unit that computes the ACC command and interfaces with the radar, encoders and actuators. The vehicles' physical setup is illustrated in Figure 1.

A PC-104 computer has been installed to host the developed CACC control programs and manage the information exchange with DSRC, sensors and the CAN interface. A GPS sensor with update rate of 5 Hz is included for time synchronisation and position logging. The CAN interface block has been incorporated in a Man-in-the-Middle configuration to bridge the PC-104 with the embedded ACC gateway, enabling flow of CAN messages on both directions. When the CACC control is activated, the CAN interface starts sending gateway messages to the PC-104, while overriding the embedded ACC unit messages with those coming from the PC-104. This configuration, on top of the drive-by-wire architecture, makes both acceleration and braking reachable both to the ACC gateway messages on

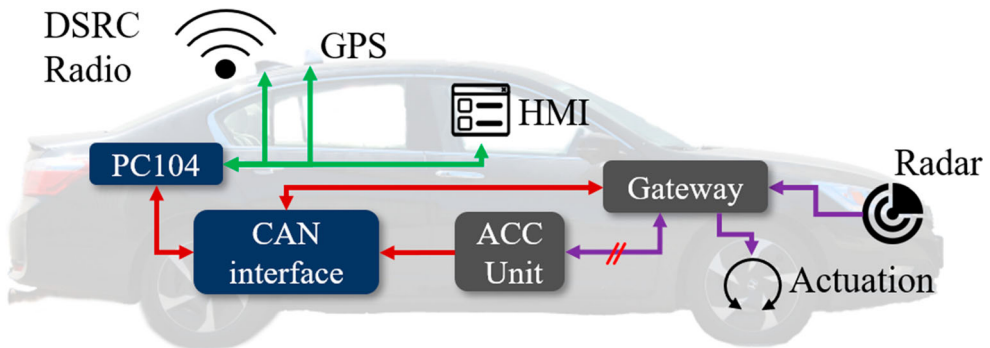
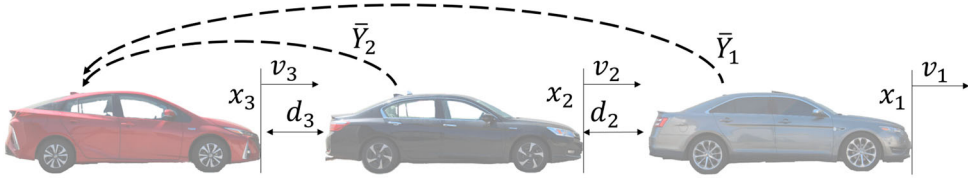


Figure 1. Physical architecture implemented on the vehicle experimental platform that enables CACC operation.

Table 1. Description of experimental platforms' features.

Vehicle	Powetrain	Mass [kg]	Power [HP]	Brake control method
2017 Toyota Prius	Hybrid Parallel	1528	121	ACC message override
2014 Honda Accord	Hybrid Serial	1723	141	Direct CAN command
2013 Ford Taurus	IC Engine	1882	240	ACC message override

**Figure 2.** Illustration of the string configuration and its variables.

every vehicle and the control generated messages. For the DSRC implementation, vehicles have been retrofitted with Cohda wireless units, providing V2V communication capabilities. A Human–Machine Interface has also been installed in the vehicle to display relevant system status cues and allow the driver to select control and gap settings on-the-fly.

The three vehicle platforms used in this work belong to the United States Argonne National Research Laboratory and their relevant information is provided below in Table 1.

Figure 2 depicts the string formation and variables description. As a matter of notation, index ‘ i ’ will refer to the ego (subject) vehicle in the i th position in a string of size n , where $i \in [1, n]$. At each time step, vehicles broadcast a set of variables \bar{Y} including states and control signals for other vehicles to listen to. The vehicle longitudinal position and velocity are denoted by x_i and v_i . The bumper-to-bumper distance d_i between ego and its preceding vehicle is given by $d_i = x_{i-1} - x_i - L_{i-1}$, where L_{i-1} is the preceding vehicle length. While variables in lower case will refer to time domain, those on upper case will refer to its corresponding frequency domain variable after applying a Laplace transformation, e.g. $X_i = \mathcal{L}\{x_i\}$.

In this work, each car-following system is designed to guarantee both individual gap regulation stability and string stability. The type of string stability sought in the design process is the strict \mathcal{L}_2 string stability [2], which states that the energy magnitude of the ego-vehicle states should be equal or less than that of its immediate predecessor vehicle. This guarantees that any speed disturbance is attenuated as it propagates in upstream direction. To satisfy this condition, the following equivalent inequalities should be satisfied:

$$\|x_i\|_{\mathcal{L}_2} \leq \|x_{i-1}\|_{\mathcal{L}_2}; \forall t > 0; i \in [1, n] \quad (1)$$

$$\|T_i(s)\|_{\mathcal{H}_\infty} = \left\| \frac{X_i}{X_{i-1}} \right\|_{\infty} \leq 1; \forall s > 0; i \in [1, n] \quad (2)$$

where $i = 1$ is the leader vehicle. The term $T_i(s)$ represents the propagation function from preceding vehicle's position towards the ego-vehicle position evolution. Vehicle position is used for its convenience on mixed vehicle type analyses, agreeing with the conclusions derived from GCDC [10]. Strict \mathcal{L}_2 string stability requirement is used in this work over alternatives such as head-to-tail string stability or bounded string stability, since it ensures that any disturbance caused by other vehicles than the leader, e.g. non-equipped car cuts

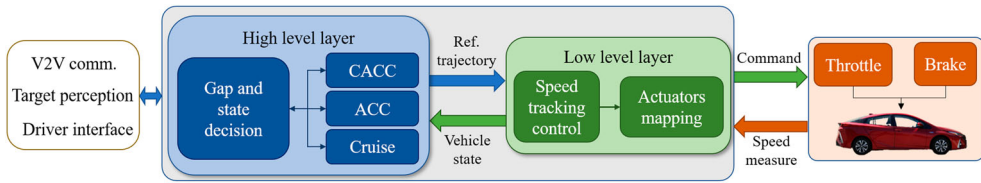


Figure 3. Graphical representation of the proposed architecture that enables CACC operation.

in at any position in the CACC string splitting the formation, will decay as it propagates, regardless the vehicle that becomes the new leader.

3. Hierarchical generic control architecture

The control architecture represents the non-physical framework of the proposed CACC system. Figure 3 illustrates the architecture as a light gray box, with both its subcomponents and data flow. It is hierarchically structured as two layers which are colour coded in blue and green, for high and low levels, respectively. These layers operate in a control loop. The high-level layer is designed for nominal operation in either Cruise Control (CC), ACC or CACC mode. It also handles communication losses, online gap settings changes, target vehicle detection interruption and cutting-in vehicles. It processes the output of target tracking system, information exchanged via V2V communication and vehicle state to regulate the distance gap towards the preceding vehicle. In this structure, the low-level layer uses the error between reference speed trajectory from the high-level and vehicle real speed to command the vehicle actuators and track such reference.

3.1. Low-level speed tracking

This layer frames the algorithms that deal with the controlled vehicle dynamics and its actuators. It is in charge of commanding the vehicle actuators and control the longitudinal dynamics given the reference speed received from the high-level layer. The design requirements set for the structure configuration are:

- Consistent speed response dynamics regardless the actuator that closes the loop
- Robust tracking with fast transient dynamics
- No overshoot in the speed response
- Adaptability to any type of vehicle dynamics and powertrains.

The structure of a vehicle of index ' i ' depicted in Figure 4 is proposed to fulfil these requirements. The velocity error $e_{v,i}$ from received reference speed $v_{ref,i}$ and the measured speed v_i is fed to the controller $C_{ll,i}$. This controller is designed to generate the desired acceleration $a_{ref,i}$ to correct the speed error. Actuator mappings are used to yield the ideal throttle or brake application in function of the measured speed and desired acceleration.

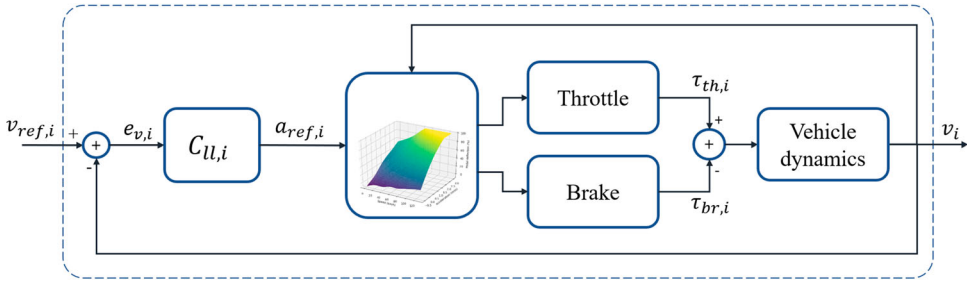


Figure 4. Block diagram of low-level structure.

3.1.1. Actuators modelling

The use of this mapping strategy is a data-driven approach that models accurately the internal powertrain and vehicle dynamics with respect to actuators application. Its purpose is to provide an instantaneous estimation of the ideal actuator application level that yields a desired acceleration, given the current vehicle speed. It consists of a look-up table represented as a 3D surface, where every reference acceleration/longitudinal speed tuple, i.e. $(a_{ref,i}, v_i)$ is mapped to either a throttle or brake application level. The following vehicle longitudinal dynamics model [22] is used during the maps estimation:

$$M_v \dot{v}_i(t) = F_{th}(t) - F_{br}(t) - 0.5\rho A_f C_d v_i(t)^2 - M_v g(\sin(\theta_r) + C_r \cos(\theta_r)); \quad (3)$$

where M_v , A_f , C_d , C_r are the vehicle mass, front area, aerodynamic coefficient and rolling resistance coefficient, respectively. F_{th} and F_{br} denote the forces applied by the powertrain and braking system over the vehicle chassis. The road inclination is referred as θ_r . The throttle or accelerator maps are built for the three vehicle platforms using a dynamometer testing setup and following these steps:

- (1) The vehicles are taken to a set of different speeds and then put off gear to coast-down to zero speed. The vehicle pitch angle is kept at $\theta_r = 0$. The obtained set of speed trajectories is used to fit the parameters of model in Equation (3) as a second-order polynomial of $v_i(t)$. Each vehicle's model is loaded to the dynamometer.
- (2) Different standard¹ and non-standard driving schedules are inputted to the vehicle in the dynamometer. Extensive acceleration, speed and throttle application level data are obtained and recorded.
- (3) All collected data points that match their speed and acceleration fields are averaged to smooth the resulting dataset. Finally, the speed vs. acceleration plane is gridded in intervals of 0.05 m/s^2 and 0.28 m/s , defining a look-up table for the throttle application values. If a grid point is not represented by any point in the dataset, the closest points are linearly interpolated to approximate the surface in Figure 5(a).

Regarding the brake actuator mapping, a similar approach is performed only for the Honda Accord. For the other vehicle platforms, the desired deceleration is tracked directly by the vehicle commercial ACC system. The same longitudinal model is loaded for each vehicle and different constant braking levels are applied from different starting vehicle speeds. This provides a set of velocity and acceleration trajectories for braking levels from

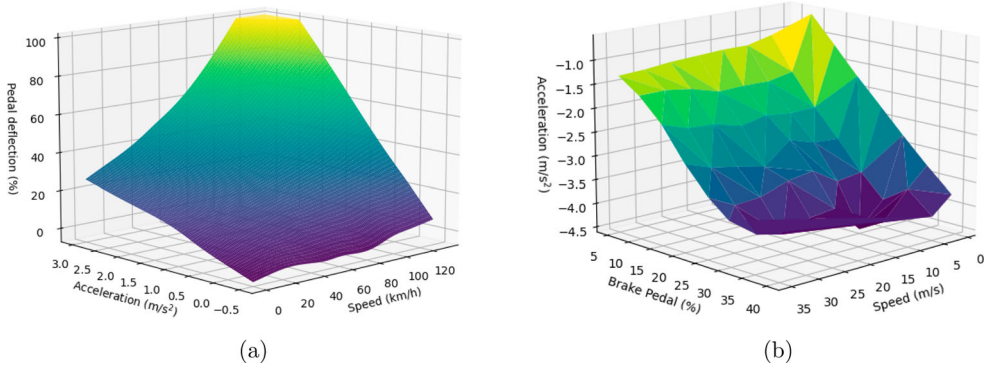


Figure 5. Illustration of actuators mappings for Honda Accord platform.

0% to 40% in steps of 5%. Experiments were truncated at 40% due to wheel blocking. As depicted in Figure 5(b), a surface is obtained that provides the expected acceleration for a given speed and braking level. The acceleration performance is observed to be almost invariant to speed, allowing to simplify the mapping from a look-up table to a fitted linear function that maps an acceleration to braking level.

3.1.2. Closed-loop characterisation

Once the actuator mappings are loaded in the vehicles, a reference acceleration profile is designed to excite the vehicle longitudinal dynamics in open loop. Such acceleration profile is passed through the maps to record the vehicles' longitudinal speed evolution. The speed responses with respect to desired acceleration are approximated to a linear transfer function with an integrator and a pole in the left half plane to approximate transient dynamics. Given the fast response and accuracy enabled by the actuators' maps, a classical proportional controller structure is chosen for $C_{ll,i}$ to control the speed error $e_{v,i}$. The gain is adjusted for each vehicle following the design objectives stated above, which translate to phase margin, bandwidth and overshoot specifications. Finally, after tuning the controller gains for each of vehicles' speed tracking systems, a reference speed profile is set to visualise vehicles low-level speed tracking responses. In Figure 6, the time and frequency responses of low-level speed tracking modules are presented for the three platforms. In the left figure, the responses to a series of speed steps are presented.

The three vehicles react fast with little to no overshoot and are able to track changes accurately. Despite the difference in powertrains, one can see that all vehicles respond with very similar transient time, only the Ford Taurus shows a shorter bandwidth. This can be due to the larger rotational inertia from the Taurus transmission, compared to the vehicles with faster electrically assisted propulsion. One benefit of this approach is that acceleration and braking responses result highly similar and consistent, guaranteeing that a second-order model of the form:

$$G_i(s) = \frac{V_i}{V_{ref,i}} = \frac{\omega_{n,i}^2}{s^2 + 2\xi_i\omega_{n,i}s + \omega_{n,i}^2} \quad (4)$$

describes the low-level speed tracking dynamics without loss of accuracy, where $\omega_{n,i}$ and ξ_i are the natural frequency and damping factor. The frequency responses of the captured

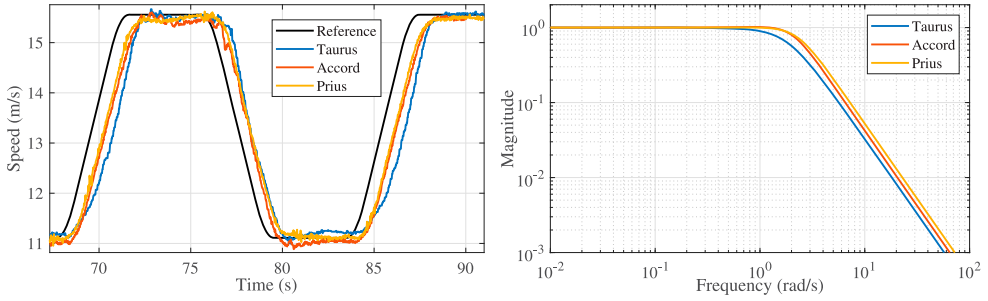


Figure 6. Low-level speed tracking systems time (left plot) and frequency (right plot) for the three vehicle platforms.

models are depicted as those in right plot in Figure 6. The design process of high-level layer is centred on this model structure to guarantee the expected performance.

3.2. High-level gap control

The reference speed is generated by the high-level control layer, which regulates the distance gap towards the preceding vehicle, for ACC and CACC vehicles. The main objective of this structure is to enable safe car-following operation in highway and real traffic scenarios. Three modes are disposed in the high-level layer on a finite-state machine setup: CC, ACC and CACC. If no preceding vehicle is detected, the speed is smoothly increased and saturated at the road speed limit. In CC mode, if a vehicle is detected within a range between once to twice the ACC target time gap h_{ACC} , the relative speed is penalised with a proportional controller. This guarantees a smooth coupling from CC to ACC when the vehicle enters the h_{ACC} region. If preceding vehicle cuts out of the subject lane, or increases the gap beyond $2h_{ACC}$, the vehicle switches to track the road speed limit. When the ego-vehicle is coupled in ACC mode, the driver is allowed to upgrade to CACC mode. To allow this, the DSRC communication link must be confirmed with the nominal latency and the target perception tracking must be detected stable. If the DSRC is interrupted or lost for a period larger than a tolerance time, the system is smoothly switched back to ACC. All transitions between operation modes are planned constraining the vehicle acceleration and jerk to guarantee comfortable driving.

The control architecture that enables CACC is represented as a block diagram in Figure 7. The term ‘ s ’ denotes the Laplace operator for time differentiation. This two degree-of-freedom structure accounts with feedback and feedforward systems that are designed complementarily. An LPF structure is adopted that uses reference velocities of leader and preceding vehicles in feedforward. These types of structures have proven to increase significantly the string performance [23]. Two feedforward systems implemented, $F_{i,i-1}(s)$ and $F_{i,1}(s)$, which process the received signals of preceding and leader vehicles, respectively. Their outputs are added to yield the feedforward output $U_{ff,i}$. Notice that signals received via V2V links are delayed by $D(s) = e^{-\theta s}$ where θ is the node-to-node communication time delay, usually no more than 0.1s. The feedback system $C_i(s)$ generates the feedback output $U_{fb,i}$ from the spacing error E_i between the measured gap and desired gap. This is added to the feedforward action to generate the reference velocity $V_{ref,i}$

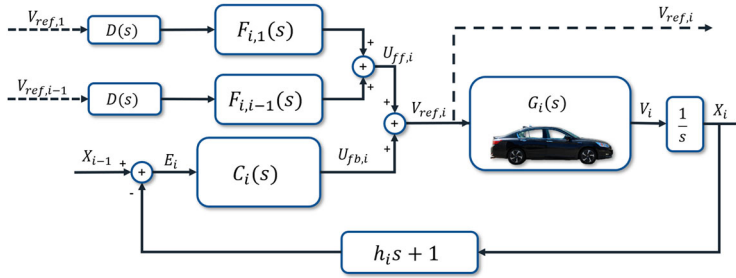


Figure 7. Feedforward/feedback control architecture for CACC operation.

sent to the low-level speed tracking layer $G_i(s)$ and also broadcasted to the other CACC vehicles. If the state machine switches to ACC, the feedforward link is removed and $V_{ref,i}$ is calculated instead by adding $U_{fb,i}$ to the measured speed V_i . The outer negative feedback loop $h_i s + 1$ (referred also as $H_i(s)$) denotes the spacing policy.

3.2.1. Spacing policy

The desired distance gap is computed from either a Constant Time Gap (CTG) or Variable Time Gap (VTG) policy. It is defined as $d_{ref,i} = r + h_i v_i$, where h_i is the desired time gap. On one hand, the CTG policy refers a distance gap that is proportional to the ego-speed added to a safety distance r . On the other hand, the VTG policy proposed in [24] modifies the desired time gap with the speed, maximising traffic throughput without degrading string stability or safety.

The VTG policy defines a speed threshold v_{lim} to divide the full speed range in urban and highway speeds. For this topology, the time gap h_i becomes function of the vehicle speed and is increased linearly from an initial value h_{min} to target value h_{max} that is kept constant for $v_i \geq v_{lim}$. This policy leverages the time gap transition to yield shorter distance gaps at higher speeds, increasing traffic throughput while maintaining safe gaps and the same dynamics than CTG.

The design of VTG policy must consider the vehicles physical capabilities to ensure safe operation. In [24], the minimal distance to be kept is calculated studying the car-following kinematics of a braking manoeuvre performed by the preceding vehicle. The cited study is extended in this work by removing the vehicles' homogeneity assumption by considering the difference between vehicles' braking capabilities. The minimal safe distance $d_{min,i}(v_i)$ results a second degree polynomial in function of the ego-vehicle speed, assuming that the manoeuvre occurs at equilibrium, i.e. $v_i \approx v_{i-1}$:

$$d_{min,i}(v_i) = \theta v_i + \frac{v_i B_{max,i}}{J_{max,i}} - \frac{B_{max,i}^3}{6J_{max,i}^2} + \frac{v_i^2}{2B_{max,i}} - \frac{v_i B_{max,i-1}}{2J_{max,i-1}} + \frac{B_{max,i-1}^3}{8J_{max,i-1}^2} - \frac{v_i^2}{2B_{max,i-1}}; \quad (5)$$

Terms $B_{max,i}$, $B_{max,i-1}$, $J_{max,i}$, $J_{max,i-1}$ correspond to the ego-vehicle maximum deceleration, preceding vehicle maximum deceleration, ego-vehicle maximum jerk and preceding vehicle maximum jerk, respectively. Therefore, the estimation of $d_{min,i}(v_i)$ sets a lower bound on $d_{ref,i}$, which is used as a constraint in the design of the spacing policy parameters to ensure safety.

3.2.2. Feedback controller

The feedback system enforces the spacing policy and provides the required car-following loop stability. It receives the distance gap error to generate the feedback correction. The control design objectives for this structure are as follows:

- (1) Guarantee of strict \mathcal{L}_2 string stability, attenuating forward vehicles' states energy, i.e. $\|T_i(s)\|_\infty \leq 1$
- (2) Good disturbance rejection and individual loop stability despite modelling uncertainties
- (3) Optimised control effort to ensure smooth command and avoid saturations
- (4) Adaptability to real-time changes of target time gap, keeping design requirements.

The feedback system fulfils this via a Linear Parameter Varying (LPV) structure. An LPV structure is designed for each vehicle, since it is optimised for each low-level dynamics. This approach defines a grid of control polytopes placed on different operation point. The operation points are attached to a time gap value, also referred as the scheduling parameter. All polytopes process the error E_i and their outputs are linearly interpolated in function of their assigned operation points and the current scheduling parameter $h(t)$. All controllers in the grid are set with the structure of a lead compensator with cutoff of the form:

$$C_i(s) = K \cdot \frac{(1 + s/\omega_z)}{(1 + s/\omega_{p1})(1 + s/\omega_{p2})}; K, \omega_z, \omega_{p1}, \omega_{p2} > 0 \quad (6)$$

having the DC gain K , zero frequency ω_z and poles ω_{p1} , ω_{p2} as design parameters. The advantages of this structure are: (1) increased stability due to positive phase contribution, (2) no additional poles at origin and (3) attenuation of high frequencies to reject noise and avoid saturation. Each controller must yield no closed-loop poles on the right half plane and minimise the following cost function:

$$J(h) = \|W_T(s)^{-1}T(s) + W_S(s)^{-1}S(s) + W_U(s)^{-1}R(s)\|_{\mathcal{H}_\infty}; \quad (7)$$

where the closed-loop functions are derived from structure in Figure 7. At this stage, the focus is put on the feedback system contribution, so a PF topology with homogeneous string dynamics is assumed for feedback evaluation purposes, i.e. $F_{i,1}(s) = 0$ and $F_{i,i-1} = H(s)^{-1}$. For the controllers' parameters design, a robust optimal control method is applied, analysing the closed-loop functions:

$$T_i(s) = \frac{X_i}{X_{i-1}} = \frac{s \cdot F_{i,i-1}(s)D(s) + G_i(s)C_i(s)}{s + G_i(s)C_i(s)H_i(s)}; \quad (8)$$

$$S_i(s) = \frac{E_i}{X_{i-1}} = \frac{s}{s + G_i(s)C_i(s)H_i(s)}; \quad (9)$$

$$R_i(s) = \frac{U_{fb,i}}{X_{i-1}} = \frac{s \cdot C_i(s)}{s + G_i(s)C_i(s)H_i(s)}; \quad (10)$$

The cost function in Equation (7) serves to quantify the resulting closed-loop functions optimality in Equation (8), given a desired time gap, candidate controller and a set of filters

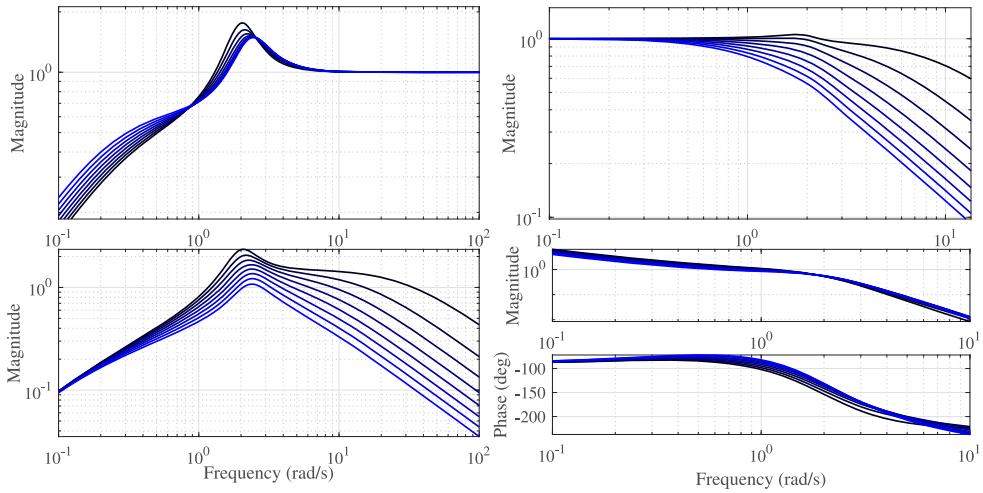


Figure 8. Magnitude of resulting closed-loop functions $S_i(s)$ (upper left plot), $T_i(s)$ (upper right plot), $R_i(s)$ (lower left plot) and bode plot of open-loop response (right lower plot). Desired time gap is increased as $h \in [0.1, 0.8]s$, shifting from black to blue lines, respectively.

that serve as a frequency response template:

$$W_T(s) = \left(\frac{h_k \cdot s/1000 + 1}{h_k s + 1} \right); \quad (11)$$

$$W_S(s) = 10^{-4} \left(\frac{100s + 1}{1/T_k + s/M_s} \right); \quad (12)$$

$$W_U(s) = 0.5 \left(\frac{h_k \cdot s/100 + 1}{0.5h_k s + 1} \right); \quad (13)$$

where h_k is the desired time gap assigned to each controller polytope $k \in [1, m]$ and m is the total amount of grid controllers. The sensitivity template peak value M_s is adapted in function of the degree of robustness expected from the system. Finally, the cost function $J(h)$ is minimised for each operation point and the template filters on Equation (11) shape the functions on Equation (8). As an example, Figure 8 shows the frequency responses of the resulting closed-loop functions after executing the design algorithm for the Honda Accord platform dynamics.

For this study, communication time delay value is taken from earlier experiments measuring end-to-end packet delivery time, showing an average delay of $\theta = 0.03$ s. For the disturbance sensitivity, the peak value is observed robust to variations in the time gap, proving good stability for the desired time gap range. The complementary sensitivity function results in a form of low-pass filter as expected, and its ∞ -norm decreases as the desired time gap value is increased. $R_i(s)$ shows a band-pass filter shape, where the feedback control acts mainly on middle frequencies. Higher frequencies are attenuated to reject noise and avoid saturation, whereas tracking at lower frequencies is handled by the feedforward link. The open-loop response given by $G_i(s)C_i(s)H_i(s)/s$ is observed stable with a phase margin that slightly decreases at shorter time gaps, due to the larger response bandwidth required. Overall, the design requirements are satisfied. However, the feedforward system

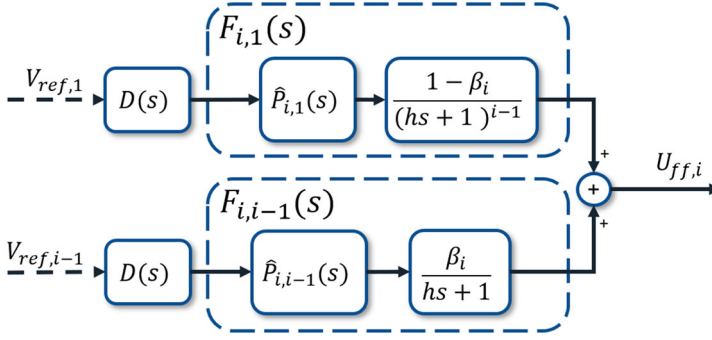


Figure 9. Block diagram of feedforward system for vehicles of index $i \geq 3$.

is in charge of guaranteeing that these are still met when relaxing the taken assumptions and considering dynamics heterogeneity with different communication topologies.

3.2.3. Feedforward system

The feedforward system enhances the reference tracking performance. It leverages the received information from forward vehicles via V2V links to increase the system string stability. The structure of feedforward system $F_i(s)$ is detailed in Figure 9.

The term $\hat{P}_{i,i-1}(s)$ denotes the ratio $\frac{\hat{G}_{i-1}(s)}{\hat{G}_i(s)}$, where \hat{G}_i represents the low-level dynamics of the i th vehicle approximated to the structure given in Equation (4). Notice that the feedforward system implements an LPF topology, using reference speeds from leader and predecessor vehicles. This topology is motivated by the increase of reaction speed provided by the use of leader vehicle information. For vehicle $i = 2$, leader and preceding are the same vehicle, so PF strategy is performed. As depicted in Figure 9, the system has two branches, one for each vehicle signal received. Each branch has two stages or sub-blocks. The first stage concerns the dynamics heterogeneity between connected vehicles by processing the received reference speed with the ratio of both vehicles' estimated low-level dynamics (leader-ego or preceding-ego). The second sub-block low-pass filters the processed signal in function of the desired time gap and vehicle position in the string. The parameter $\beta_i \in (0, 1)$ is tuned following the guidelines proposed in [18]. These state that vehicles with shorter response bandwidth that their predecessors should leverage leader information more than vehicles with faster response times, increasing their reaction speed capabilities.

For this work, low-level dynamics models have been identified from experimental results and loaded on every vehicle in the string. If prior knowledge of other vehicles low-level dynamics' is not available, dynamics can be identified online by implementing the algorithm in [25]. Consideration of string heterogeneity and use of leader vehicle information make the string stability study more complex than PF topologies, yielding a vehicle position evolution that is described by

$$X_i = \frac{sF_{i,i-1}(s)D(s)\frac{G_i(s)}{G_{i-1}(s)} + C_i(s)G_i(s)}{s + C_i(s)G_i(s)H(s)}X_{i-1} + \frac{F_{i,1}(s)D(s)G_i(s)}{s + C_i(s)G_i(s)H(s)}V_{ref,1}. \quad (14)$$

However, the closed-loop analysis requires to study the transfer function $\frac{X_i}{X_{i-1}}$. Knowing that the string of vehicles acts as an interconnected system, X_{i-1} is developed in function of the leader position evolution X_1 as

$$X_{i-1} = \frac{X_{i-1}}{X_{i-2}} \frac{X_{i-2}}{X_{i-3}} \cdots \frac{X_2}{X_1} X_1; \quad (15)$$

$$X_{i-1} = T_{i-1}(s) T_{i-2}(s) \cdots T_2(s) X_1. \quad (16)$$

Given that $X_1 = G_1(s) V_{ref,1}/s$, and assuming all vehicles implement the same desired time gap h , a direct relationship between X_{i-1} and X_1 can be traced since the transfer functions $T_i(s)$ can be approximated to $D(s)H_i(s)^{-1}$. This holds for strings with time gap-based policies, demonstrated on CACC experimental results and conclusions from [26]. Assuming this, and mixing Equations (14) and (15), one obtains

$$X_i = \frac{sD(s)F_{i,i-1}(s)\frac{G_i(s)}{G_{i-1}(s)} + sD(s)\left(\frac{D(s)}{H(s)}\right)^{i-2}F_{i,1}(s)\frac{G_i(s)}{G_1(s)} + G_i(s)C_i(s)}{s + G_i(s)C_i(s)H_i(s)} X_{i-1}; \quad (17)$$

$$X_i = \frac{s\beta_i D(s)\Delta P_{i,i-1}(s) + s(1 - \beta_i)D(s)^{i-1}\Delta P_{i,1}(s) + G_i(s)C_i(s)H_i(s)}{s + G_i(s)C_i(s)H_i(s)} X_{i-1}; \quad (18)$$

which results in a closed form of $T_{i,i-1}(s)$ function. The term $\Delta P_{i,i-1}(s) = \frac{\hat{P}_{i,i-1}(s)}{P_{i,i-1}(s)}$ denotes the relation between estimated low-level dynamics ratio and the ground truth low-level dynamics ratio. Ideally, $\Delta P_{i,i-1}(s)$ should converge to 1 over all frequencies. Nevertheless, in case that modelling uncertainties deviate $\Delta P_{i,i-1}(s)$ or $\Delta P_{i,1}(s)$ from the expected value, the feedback structure would reject the disturbances introduced in the loop.

CACC communication links are prone to transmission delays referenced as $D(s)$ that degrade the string stability. String stability can still be guaranteed despite these delays if the expected closed-loop response bandwidth is reduced, increasing the desired time gap h . This defines a lower bound on the possible values for h , for a set of possible communication delays θ , where string stability is guaranteed for time gap values above such bound. Figure 10 illustrates this study for each of the three platforms and their designed feedback controllers. In the left figure, the study is executed for both PF topology (implemented on vehicle $i = 2$) and LPF topology (for $i = 3$).

Each curve represents the minimum desired time gap that must be set for each vehicle to guarantee string stable CACC. The minimum h is observed to increase quadratically with the communication delay, showing that greater gaps are required for larger V2V latencies. The vehicles with larger response bandwidths and more aggressive control parameters maintain string stability for shorter minimum h . Among the two topologies studied, the LPF provides a larger string stability region due to the enhanced reaction capabilities gained with the use of leader vehicle information directly.

As a general guideline, given the heterogeneous dynamics faced on mixed strings, it is important to functionally arrange the vehicles in the string. If possible, slower vehicles, or with shorter response bandwidth, should be placed in downstream positions and gradually increase the vehicles' response capabilities as their index i increments. Otherwise, the

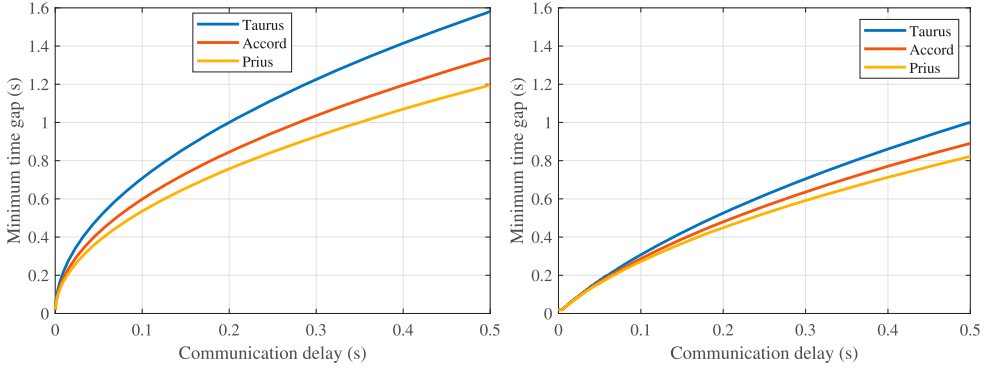


Figure 10. Minimum time gap that ensures theoretical string stability for given communication delays using PF (left figure) and LPF (right figure) topologies.

control effort will be saturated for less capable vehicles, hindering them to track oscillations from faster vehicles and possibly leading to rear-end collisions. This strategic string ordering also avoids that systems $F_{i,1}(s)$ and $F_{i,i-1}(s)$ develop an overshoot on their spectral shape, amplifying the V2V signals due to the form of $\hat{P}_{i,1}(s)$ and $\hat{P}_{i,i-1}(s)$.

4. Gap management strategy

The presented architecture implements CACC despite string heterogeneity. Nonetheless, it must support flexible gap settings to enable operation on real highway traffic scenarios. Cut-in from other vehicle is also a challenge that remains to be solved to further encourage adoption of CACC systems on public roads. A gap management system is proposed that uses a motion planning algorithm to handle both gap settings changes and cutting in/out vehicles in highway operation.

Initially, the subject vehicle is stable at time gap $h = h_{CACC}$ with its predecessor. Once a non-connected vehicle cuts in the gap between these two at $t = t_0$, the target perception system switches to track the vehicle, which is detected at a gap of h_{init} seconds. The car-following system immediately switches from CACC to ACC and sets the desired time gap as $h = h_{init}$, avoiding aggressive or jerky control. Subsequently, the ego-vehicle increases smoothly the desired gap towards the ACC time gap $h = h_{ACC}$. In the same way, if the non-connected vehicle cuts out of the subject lane, the ego-vehicle will remain in ACC mode while closing the existing gap with respect to the previous preceding vehicle. In case such preceding vehicle is compatible to perform CACC, the driver is allowed to trigger the transition to CACC if the V2V link is stable. The transition from ACC to CACC is performed smoothly and bounding the vehicle accelerations. All real-time modifications to the desired time gap are enabled by the motion planning algorithm.

4.1. Motion planning-based algorithm

This algorithm is in charge of computing the motion trajectory that the vehicle should track when the desired gap is changed, which may be triggered by either cut-in/out scenarios or a driver preferences update. It computes a time gap vector $\underline{h}(t)$ that goes from h_{init} to the

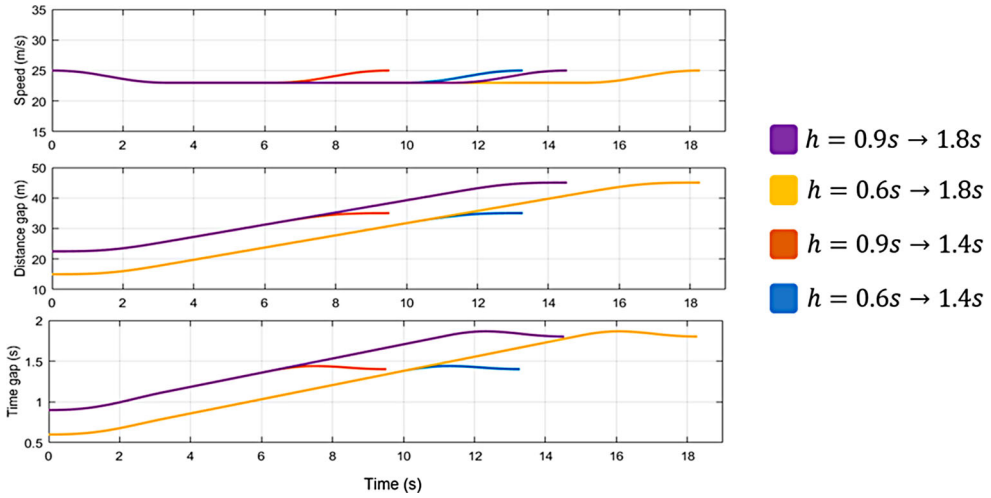


Figure 11. Speed, inter-distance and time gap trajectories for four different gap opening manoeuvres.

target value h_{targ} . It calculates an optimal speed trajectory to open or close the required gap, while constraining the longitudinal acceleration and jerk. The algorithm is as follows:

- (1) Define bounds for the planned longitudinal speed, acceleration and jerk, depending on the situation.
- (2) Estimate the initial time gap using $h_{init} = \frac{d(t_0) - r}{v_i(t_0)}$, where r , $d(t_0)$ and $v_i(t_0)$ denote the safety distance, measured distance and velocity at the manoeuvre trigger time, respectively.
- (3) Assuming that the preceding vehicle is keeping constant speed, the distance gap to be added (or reduced) to reach h_{targ} is estimated as $\Delta d = \frac{h_{targ} v_i(t_0) - r - d(t_0)}{v_i(t_0)}$.
- (4) A profile of jerk steps is planned that produces the required gap modification Δd , while guaranteeing that speed, acceleration and jerk variables remain constrained. The jerk profile is integrated twice over time to obtain a smooth longitudinal speed profile vector $\vec{v}_i(t)$.
- (5) The planned speed profile $\vec{v}_i(t)$ is used to calculate the desired time gap profile $\vec{h}(t)$ as a discretised trajectory of h that transitions from h_{init} towards h_{targ} , using the formula:

$$\vec{h}(t) = \frac{v_i(t_0)h_{init} - \int_{t_0}^t (v_i(\tau) - v_i(t_0)) d\tau}{v_i(t)}. \quad (19)$$

Figure 11 shows four different time gap trajectories that are set with the same constraints but different initial and target values, illustrating the algorithm output. The constraints are set as $|j(t)| \leq 0.8 \text{ m/s}^3$, $|a(t)| \leq 1 \text{ m/s}^2$ and $23 \text{ m/s} \leq v(t) \leq 25 \text{ m/s}$.

One can observe how the speed profile evolves smoothly from the initial speed value after increasing the distance gap. Despite the different levels of h_{init} and h_{targ} , the algorithm proves useful to generate the required gap plan. This planned time gap profile is used to adapt the spacing policy block on the outer feedback loop of structure in Figure 7. It also schedules the feedback and feedforward controllers, from $t = t_0$ until the target time gap is

reached. It is worth to mention that even if the relative speed is non-zero, since the manoeuvre is executed in closed loop, the car-following control structure will mitigate the speed error through the feedback loop.

5. Experimental results

The developed architecture has been implemented and tested on the three vehicle platforms. First, highway driving results are shown with ACC state activated. The CACC system is then tested on highway driving at high speeds with some gap setting changes to demonstrate the effectiveness of motion planning algorithm. The CACC system has also been tested on Crows Landing Airport facilities (test track), evaluating less conservative time gaps and demonstrating the full performance of the proposed architecture with VTG policy. Finally, the manoeuvring of cut-in and out situations is demonstrated with experiments on such test track.

5.1. ACC car-following results

The ACC structure has been set on the Toyota Prius platform and evaluated on highway I-80 with public traffic. Results are depicted in Figure 12. Upper plot shows target and subject vehicle speeds. Lower left plot shows the ACC spacing error, and lower right plot shows the target and measured time gap. The controlled vehicle tracks very accurately all the speed variations from the target vehicle, which is manually driven.

The control design, together with a sufficiently large time gap (1.3 s), demonstrates that speed variations are smoothly tracked without overshoots. It is also visible that the speed propagation from target to ego-vehicle is uniform and robust to different levels of acceleration and braking, which was one of the proposed design objectives. The time gap is seen to be accurately tracked and the absolute spacing error deviates three meters at most ($t = 500$ s), which is acceptable given the limitations of ACC systems.

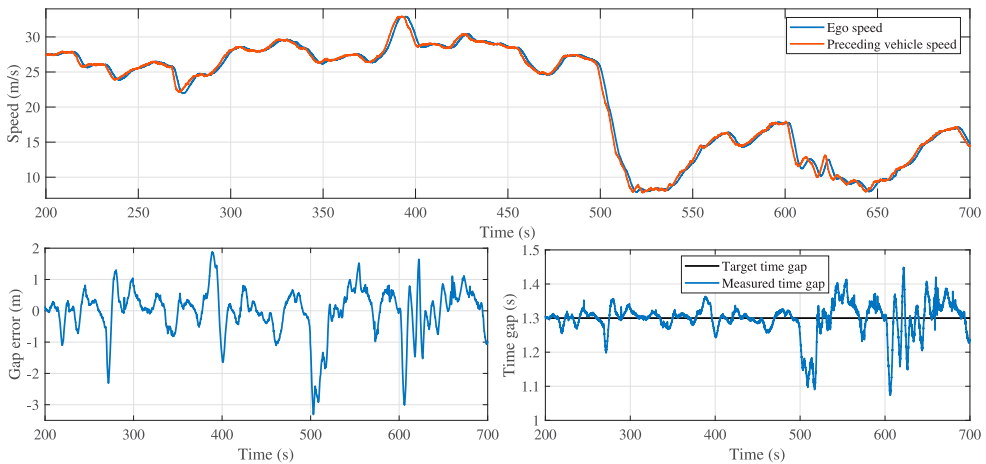


Figure 12. ACC car-following results in highway scenarios with real traffic.

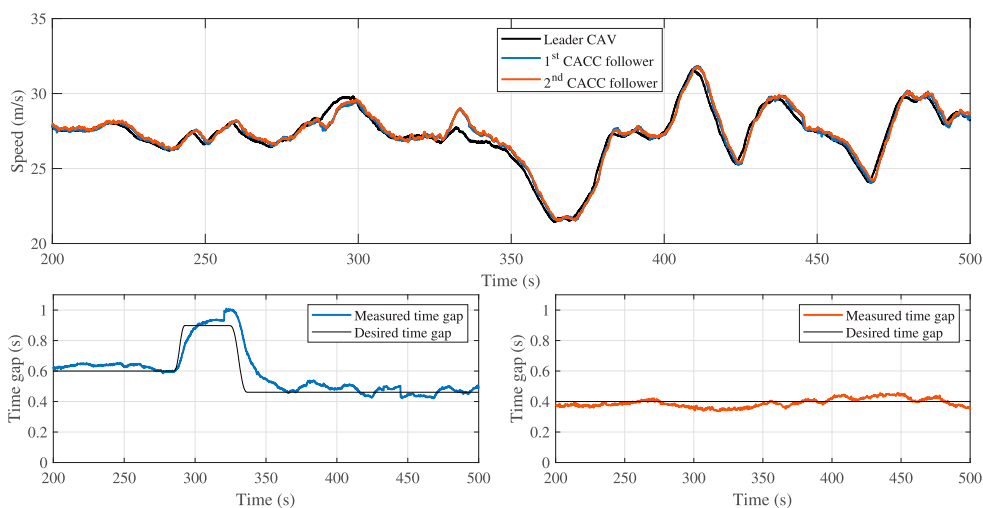


Figure 13. CACC results on highway scenarios. Speed plot (upper figure), first follower’s measured and desired time gap (lower left figure) and second follower’s measured and desired time gap (lower right plot).

5.2. CACC validation results

The three vehicles are used to validate the CACC car-following performance. On all tests, the vehicles ordering is set following the guidelines discussed in Section 3.2.3. The ideal configuration from the leader to last results: Ford Taurus, Honda Accord and Toyota Prius. Figure 13 shows the speed and time gap results for the string of vehicles driving in highway I-80. The leader vehicle is set on ACC mode, whereas the other two operate on CACC.

The two CACC followers are observed to track accurately the speed variations of leader vehicle due to external traffic disturbances, forcing different levels of acceleration and braking. The first follower changes its desired time gap twice, the first increasing 0.3 s ($t = 285$ s) and the second reducing 0.4 s ($t = 325$ s). This online gap changes are visible in the speed changes of the first follower, producing a speed difference that allows to track the desired gap changes generated by its motion-planning algorithm. The second vehicle follower keeps $h = 0.4$ s in spite of the downstream oscillations, it is observed to maintain the required distance. Comparing to the ACC experiments, it is visible in the spacing error evolution indicated that the tracking is greatly enhanced when upgrading from ACC to CACC.

Closed test track results have been conducted to evaluate the performance limit manoeuvres on public road. A multisine speed profile is designed for the leader vehicle that results from adding random phase sine signals of different frequencies. The sines amplitudes and frequencies have been selected to excite the expected frequency region that allows to study the string stability. The CACC followers have been set on VTG with $h_{min} = 0.05$ s, $h_{max} = 0.2$ s and $v_{lim} = 18$ m/s. Toyota Prius and Honda Accord vehicles have been interchanged of positions, now having $i = 2$ and $i = 3$, respectively. This allows to test the system robustness to different string configurations. Figure 14 depicts the experiment results, showing vehicles’ speeds, spacing error and target time gap.

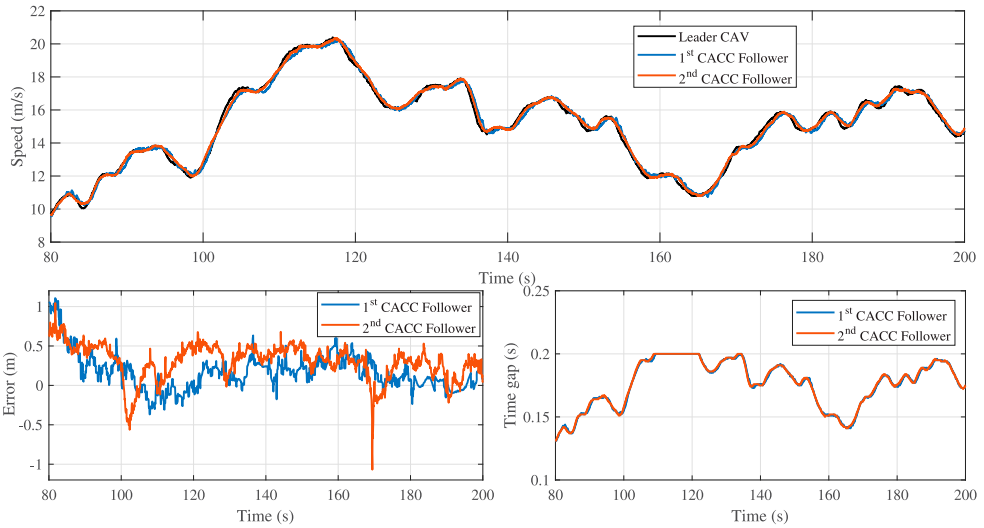


Figure 14. CACC experiment in test tracks using the VTG policy and modifying the vehicles ordering.

This experiment illustrates that despite more exigent gap settings, the CACC system still provides string stable performance, given that oscillations decrease upstream. The followers track more closely the speed changes, demonstrating the potential of the low-level speed tracking layer to yield consistent dynamics. The spacing error remains within acceptable bounds (mostly below 0.5 m), also guaranteeing that the reference time gap is closely tracked, as the lower right figure shows. The desired time gap is observed to evolve in function of the longitudinal speeds as a consequence of the VTG policy, yielding shorter inter-vehicle distance and potentially increasing traffic throughput.

The last experiment evaluates cut-in situations handling (Figure 15). A string of two CACC vehicles (Ford Taurus and Toyota Prius) is set with the leader driving at a constant speed, whereas a third vehicle is manually driven. The desired time gap for ACC is $h = 1.35$ s and $h = 0.9$ s for CACC. First, the string vehicles are stable in CACC mode and at $t = 68$ s, the non-connected vehicle cuts between both vehicles. The state machine switches immediately to ACC car-following and executes the motion planning algorithm to estimate the time gap profile from $h_{init} = 0.207$ s to $h_{targ} = 1.35$ s. This profile is set to the ACC structure and the gap-opening manoeuvre is performed by introducing some positive relative speed smoothly during approximately 10 s. Both ACC and CACC structures are running in parallel at all times, which allow to switch from one to the other if required. One can see in the ACC gap error that the time gap profile generated to open the required gap is tracked accurately, which is also notable in the measured time gap evolution. After ending the gap-opening manoeuvre, the non-CACC vehicle speed variations are tracked. At $t = 86$ s, the non-CACC vehicle cuts out of the formation and the gap management system estimates another time gap profile to perform the gap-closing manoeuvre. Such manoeuvre induces the ego-vehicle to speed up and transition from $h = 2.45$ s back to $h = 1.35$ s. Once stable at ACC car-following, the driver triggers the transition to CACC at $t = 100$ s, forcing a negative relative speed with respect to the CACC leader and moving

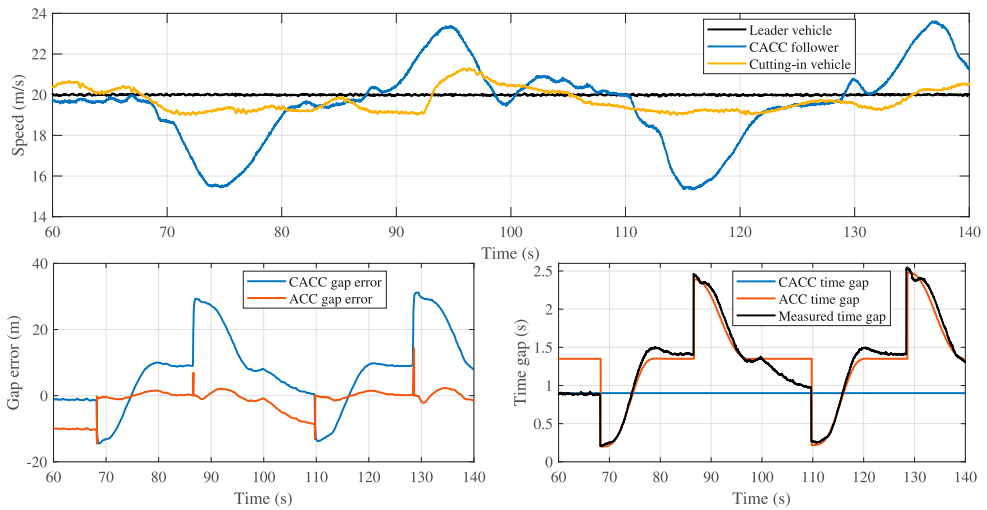


Figure 15. Speeds evolution of leader, CACC follower and cutting-in vehicle (upper plot), ACC and CACC spacing errors (lower left plot), and ACC, CACC and measured time gap (lower right plot).

from $h = 1.35$ s to $h = 0.9$ s. Just when the switching is completed, the non-CACC vehicle cuts-in again and the described process is repeated.

6. Concluding remarks

This paper introduced an architecture that enables CACC car-following on vehicles of different dynamics and powertrains. The architecture also allows operation in CC and ACC, which is fundamental to guarantee safety in case of communication faults or cut-in vehicles. The proposed CACC structure is hierarchically composed by a high-level layer that regulates the car-following kinematics, and a low-level layer that deals with the vehicle control actuation and powertrain dynamics to track a given reference speed. A feedback loop is used that relies on actuator mappings to provide an accurate actuation level in function of the current speed and desired acceleration. A feedforward/feedback structure is used in the high-level layer. The feedforward system processes the V2V information to increase the reference tracking capabilities and deal with the string heterogeneity. The feedback system is designed as an LPV structure, which is composed of a grid of optimally designed robust controllers scheduled by the desired time gap. On top of this, a gap management system has been designed that relies on a motion planning algorithm to generate a time gap profile vector. This allows to handle not only real-time changes in gap settings but also cut-in/out situations. The effectiveness of ACC and CACC structures has been demonstrated through both highway and tests. In addition, the performance limits of the CACC algorithm have been on different situations, gaps settings and configurations.

This work presented a promising solution to the constraint of vehicle dynamics homogeneity in CACC strings. It has been demonstrated that a consistent and predictable low-level speed tracking response is fundamental to achieve high performance strings. In spite of different powertrains, the same approach can be applied for any vehicle type. It has been observed that ICE vehicles may present slower acceleration dynamics than those with

hybrid or electric powertrains, due to larger rotational inertia of ICE vehicles' transmission. The faster response of electric motors also contributes to a relative larger response bandwidth. Regarding string stability, two main remarks can be made. (1) The strategic ordering of vehicles, increasing their response bandwidth in upstream direction, has been observed to not only impact positively on the string performance but also increase safety and reduce risk of control saturation. (2) Using the leader vehicle information in feedforward improves the string stability performance, by reducing response time and coupling faster vehicles more to their predecessors, while slower vehicles give more weight to the leader signal. The benefits of a time gap-scheduled LPV feedback structure are visible, mostly in the adaptability of the control structure to real-time changes in gap settings due to external factors. In the same line, the gap management strategy has been proved useful to yield comfortable and safe manoeuvres.

As future work, vehicles other than passenger cars, e.g. buses or heavy duty trucks, will be considered and tested with the proposed algorithm. Other types of applications such as platoon merging or emergency braking will also be considered within this framework. Traffic shockwave damping will also be studied to see the potential benefits of the proposed architecture in dealing with mixed traffic of ACC/CACC vehicles and human driven vehicles for traffic flow improvement.

Note

1. <https://www.epa.gov/vehicle-and-fuel-emissions-testing/dynamometer-drive-schedules>

Acknowledgments

The authors would like to thank Dr. Hao Liu for its support in the experimental testing of the developed work.

Disclosure statement

No potential conflict of interest was reported by the author(s).

Funding

This research was supported by the U.S. Department of Energy (DOE) Vehicle Technologies Office (VTO) under the Systems and Modeling for Accelerated Research in Transportation (SMART) Mobility Laboratory Consortium, an initiative of the Energy Efficient Mobility Systems (EEMS) Program under the direction of Mr. David Anderson, with support of the Project Manager Erin Boyd and Danielle Chou who are gratefully acknowledged.

References

- [1] Gunter G, Gloudemans D, Stern RE, et al. Are commercially implemented adaptive cruise control systems string stable?. *IEEE Trans Intell Transp Syst.* 2021;22:6992–7003.
- [2] Ploeg J, Van De Wouw N, Nijmeijer H. Lp string stability of cascaded systems: application to vehicle platooning. *IEEE Trans Control Syst Technol.* 2014;22(2):786–793.
- [3] Stern RE, Cui S, Delle Monache ML, et al. Dissipation of stop-and-go waves via control of autonomous vehicles: field experiments. *Transp Res Part C: Emerg Technol.* 2018;89:205–221.
- [4] Ersal T, Kolmanovsky I, Masoud N, et al. Connected and automated road vehicles: state of the art and future challenges. *Veh Syst Dyn.* 2020;58(5):672–704.

- [5] Lu XY, Shladover S, Bergquist S. Truck cacc implementation and test to verify control performance. *Transp Res Rec.* **2019**;2673(8):353–364.
- [6] Shladover SE, Nowakowski C, Lu XY, et al. Cooperative adaptive cruise control: definitions and operating concepts. *Transp Res Rec: J Transp Res Board.* **2015**;2489:145–152.
- [7] Milanés V, Shladover SE, Spring J, et al. Cooperative adaptive cruise control in real traffic situations. *IEEE Trans Intell Transp Syst.* **2014**;15(1):296–305.
- [8] Ploeg J, Shukla DP, van de Wouw N, et al. Controller synthesis for string stability of vehicle platoons. *IEEE Trans Intell Transp Syst.* **2014**;15(2):854–865.
- [9] Liu H, Lu XY, Shladover SE. Mobility and energy consumption impacts of cooperative adaptive cruise control vehicle strings on freeway corridors. *Transp Res Rec.* **2020**;2674(9):111–123.
- [10] Wang C, Nijmeijer H. String stable heterogeneous vehicle platoon using cooperative adaptive cruise control. In: *2015 IEEE 18th International Conference on Intelligent Transportation Systems (ITSC)*, Gran Canaria, Spain. IEEE; 2015. p. 1977–1982.
- [11] Robinson T, Chan E, Coelingh E. Operating platoons on public motorways: an introduction to the sartre platooning programme. In: *17th World Congress on Intelligent Transport Systems*. Vol. 1, **2010**. p. 12.
- [12] Ploeg J, Semsar-Kazerooni E, Medina AIM, et al. Cooperative automated maneuvering at the 2016 grand cooperative driving challenge. *IEEE Trans Intell Transp Syst.* **2018**;19(4):1213–1226.
- [13] Jin IG, Avedisov SS, He CR, et al. Experimental validation of connected automated vehicle design among human-driven vehicles. *Transp Res Part C: Emerg Technol.* **2018**;91:335–352.
- [14] di Bernardo M, Salvi A, Santini S. Distributed consensus strategy for platooning of vehicles in the presence of time-varying heterogeneous communication delays. *IEEE Trans Intell Transp Syst.* *ITS America.* Montreal **2015**;16(1):102–112.
- [15] Zheng Y, Li SE, Li K, et al. Distributed model predictive control for heterogeneous vehicle platoons under unidirectional topologies. *IEEE Trans Control Syst Technol.* **2017**;25(3):899–910.
- [16] Zhu Y, Zhao D, Zhong Z. Adaptive optimal control of heterogeneous CACC system with uncertain dynamics. *IEEE Trans Control Syst Technol.* **2019**;27:1772–1779.
- [17] Navas F, Milanés V, Flores C, et al. Multi-model adaptive control for CACC applications. *IEEE Trans Intell Transp Syst.* **2020**;22:11.
- [18] Shaw E, Hedrick JK. Controller design for string stable heterogeneous vehicle strings. In: *2007 46th IEEE Conference on Decision and Control*. New Orleans, IEEE; 2007. p. 2868–2875.
- [19] Flores C, Milanés V. Fractional-order-based ACC/CACC algorithm for improving string stability. *Transp Res Part C: Emerg Technol.* **2018**;95:381–393.
- [20] Gao F, Li SE, Zheng Y, et al. Robust control of heterogeneous vehicular platoon with uncertain dynamics and communication delay. *IET Intell Transport Syst.* **2016**;10(7):503–513.
- [21] Milanés V, Shladover SE. Handling cut-in vehicles in strings of cooperative adaptive cruise control vehicles. *J Intell Transp Syst.* **2015**;20(2):178–191.
- [22] Rajamani R. *Vehicle dynamics and control*. Springer Science & Business Media; **2011**.
- [23] Peters A, Mason O, Middleton RH. *Leader following with non-homogeneous weights for control of vehicle formations*. 2016.
- [24] Flores C, Milanés V, Nashashibi F. A time gap-based spacing policy for full-range car-following. In: *2017 IEEE 20th International Conference on Intelligent Transportation Systems (ITSC)* Yokohama. IEEE; 2017. p. 1–6.
- [25] Flores C, Milanés V, Nashashibi F. Online feedforward/feedback structure adaptation for heterogeneous CACC strings. In: *2018 Annual American Control Conference (ACC)* Milwaukee. IEEE; 2018. p. 49–55.
- [26] Milanés V, Shladover SE. Modeling cooperative and autonomous adaptive cruise control dynamic responses using experimental data. *Transp Res Part C: Emerg Technol.* **2014**;48:285–300.